ACS APPLIED MATERIALS & INTERFACES

Research Article

www.acsami.org

Pretreatment Control of Carbon Nanotube Array Growth for Gas Separation: Alignment and Growth Studied Using Microscopy and Small-Angle X-ray Scattering

Xiaoshuang Yang,*[,†,‡] Lixiang Yuan,[†] Vanessa K. Peterson,[‡] Andrew I. Minett,[†] Ming Zhao,[†] Nigel Kirby,[§] Stephen Mudie,[§] and Andrew T. Harris[†]

[†]Laboratory for Sustainable Technology, School of Chemical and Biomolecular Engineering, Building J01, University of Sydney, NSW 2006, Australia

[‡]Australian Nuclear Science and Technology Organisation, Lucas Heights, NSW 2234, Australia

[§]Australian Synchrotron, Clayton, Victoria 3168, Australia

ABSTRACT: Aligned multiwalled carbon nanotube (CNT) arrays were prepared using chemical vapor deposition of C_2H_4 on Fe catalyst at 750 °C. CNT array height and alignment depends strongly on the duration of H_2 pretreatment, with optimal height and alignment achieved using 10−15 min pretreatment. Small-angle X-ray scattering (SAXS) was used to quantify the alignment, distribution, and size of the CNTs in arrays produced from varying pretreatment times and the results correlated with microscopy measurements. SAXS analysis revealed that the higher section of the CNT arrays exhibited better alignment than the lower section. Combining these insights with transmission electron microscopy measurements of the CNT defects within each array enable a mechanism for the CNT growth to be proposed, where the loss of alignment arises from deformation of the CNTs during their growth. Gas permeation test across densified CNT arrays indicated that the alignment of the CNT array plays an important role in the gas transport, and that the gas diffusion across the well-aligned CNT arrays was enhanced by a factor of ∼45, which is much more than that across the poorly aligned CNT arrays, with an enhancement factor of ∼8.

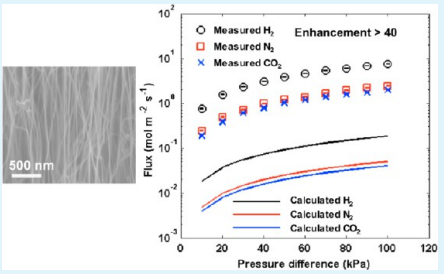

KEYWORDS: *catalysts, alignment control, growth mechanism, gas transport*

INTRODUCTION

Aligned carbon nanotube (CNT) arrays have been investigated for an extensive range of applications in the last two decades,[1−3] including for electrical applications,[4,5] as membranes for water purification,[6,7] and for DNA translocation.[8] The alignment of the CNT arrays is essential to the performance of the membrane for such applications. As a separation membrane, the CNT alignment affects the tortuosity of the membranes, which in turn influences the membrane's separation properties.[6] The CNTs in well-aligned CNT arrays have clean surfaces and strong interactions, which enable the CNTs to join end to end and form CNT yarns.[9] It is believed that the main controlling factor in the alignment of vertically grown CNTs is van der Waals forces,[4] however, there remains a lack of knowledge regarding the growth process.

The efficient synthesis of well-aligned CNT arrays has been demonstrated using chemical vapor deposition (CVD) techniques.[10,11] In the CVD process, the size and distribution of the active catalyst are reported to determine the height and alignment of the CNT array, CNT as well as wall number and diameter, with many studies focusing on catalyst preparation and pretreatment methods with the aim of controlling the CNT properties.[12,13] CNT structure and alignment within an array produced using CVD can be controlled through the duration of H_2 exposure.[14] Zhang et al.[15] and Cui et al.[16] investigated the size of catalyst particles and their interspacing under different H_2 pretreatment conditions, noting a correlation between catalyst pretreatment and CNT array height, where the interparticle distances of the catalyst controlled the confinement of the CNTs. Despite these studies, further information is required to understand the link between the CNT growth process and alignment within an array. Imperfect CNTs that contain defects on their walls are sometimes obtained during CNT growth.[17] Local deformation, occurring around a defect, can cause the CNTs to bend,[18] and it is therefore important to explore the effects of CNT defects on the alignment and growth of vertically grown CNT arrays.

The alignment of a CNT array is best investigated from a macroscopic perspective.[19] Scanning electron microscopy (SEM) and transmission electron microscopy (TEM) are the main methods used to characterize the alignment, height, and diameter of the CNTs within an array.[13,14] Both TEM and SEM yield information concerning the structure, arrangement, and alignment of the CNTs, but this information is limited to the size of the image field, which contains relatively few CNTs. As supplementary techniques to SEM and TEM, X-ray diffraction

Received: December 27, 2012
Accepted: March 21, 2013
Published: March 21, 2013

   dx.doi.org/10.1021/am3032579 | ACS Appl. Mater. Interfaces 2013, 5, 3063−3070

(XRD) and small-angle X-ray scattering (SAXS) are very useful in the structural characterization of aligned CNT arrays. Both XRD and SAXS allow information to be gained for more CNTs per measurement than from microscopy. SAXS and XRD data are obtained as a function of scattering vector, q, which is inversely related to a correlation length in the material, d, by $q = 2\pi/d$, and as such these techniques can be used to quantify the average CNT structure and degree of alignment within the part of the array that is in the beam. Using a synchrotron X-ray source allows a relatively small beam to be used, enabling this average information to be obtained as a function of position within the sample, such as array height. XRD can be used to obtain information concerning the crystal structure of aligned CNT arrays, as well as the number of layers within a CNT and the domain size of the CNTs within the array,[20] and both the tube wall distance and average wall numbers within CNTs.[21] SAXS offers insights into the bulk large-scale structure of CNT arrays, such as their alignment and density, although the length-scale of the structural information accessible using SAXS overlaps sufficiently with conventional XRD to also enable the determination of CNT diameter. Relative to SEM and TEM, SAXS and XRD probe a much larger region of the CNT array, yielding structural information for a greater number of CNTs.[19,22]

CNT arrays for this study were prepared on Fe catalyst that was annealed in H_2 for various times. SAXS was used to macroscopically assess the alignment, diameter, and distribution of the CNTs within the array as a function of the catalyst anneal time. SAXS data were obtained as a function of CNT height. TEM, SEM, and Raman measurements were employed to characterize the CNT arrays more locally than probed using SAXS, and along with Raman spectroscopy measurements, these results were used to propose a mechanism for CNT growth. Gas permeation tests were also performed on the as-prepared arrays.

EXPERIMENTAL SECTION

Ten-nanometer-thick Al_2O_3 and one-nanometer-thick Fe catalyst films were deposited on a Si wafer (p-type, 100, 0.005−0.20 ohm-cm) using electron beam evaporation (Temescal). The as-prepared catalyst-deposited wafer was cut into pieces (5 mm × 5 mm) using a diamond scribe and stored under vacuum until use.

Catalyst pretreatment and CNT growth was performed in an alumina tube furnace (GSL1300, MTI). A quartz tube (ID = 24 mm, length =150 mm) was placed into the center of the furnace and used as a sample holder. The flow rates of the gases used, Ar, H_2, and C_2H_4, were controlled by a series of mass flow controllers (Alicat Scientific 16 Series). At ambient temperature the system was flushed with 1000 standard cubic centimeters per minute (sccm) of Ar for 20 min, before the sample was heated to 750 °C in 500 sccm Ar. When 750 °C was reached, a 400/140 sccm H_2/Ar mixture was introduced and the system maintained at this temperature for 5−20 min. Following the catalyst pretreatment, a 400/140/115 sccm H_2/Ar/C_2H_4 mixture was introduced to induce CNT growth for 30 min, after which the system was cooled under a flow of 500 sccm Ar. The system was operated at atmospheric pressure. CNT arrays are referred to using the notation Tx where x denotes the time in minutes of the H_2 pretreatment and CNT arrays grown after the pretreatment times 5, 10, 15, and 20 min. A set of blank samples was prepared for analysis of the catalyst at different pretreatment times by cooling the furnace within 30 min after the H_2 pretreatment without adding C_2H_4.

Gas permeation tests were performed using particularly long CNT arrays, achieved using 120 min growth time, and synthesized using 5 and 10 min pretreatment times. The as-synthesized CNT arrays were water-etched at 750 °C and then detached from their substrates using a previously described vacuum extraction method.[23] Densified free-standing CNT arrays were produced by soaking the CNT arrays in acetone and drying them at 100 °C for 2 h, resulting in arrays that were 15% of their original size. The densified arrays were used as membranes in single-gas permeation tests by mounting them on porous gaskets (10 μm pores) using a 1/4 in. VCR fitting (Figure 1).

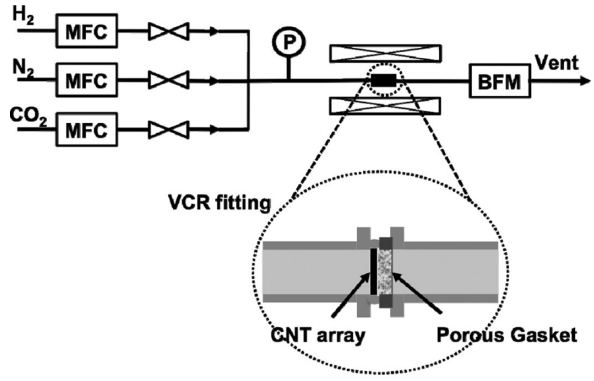

Figure 1. Schematic for the single-gas permeation tests, showing mass-flow controllers (MFC), the bubble flow meter (BFM), and the CNT arrays.

A pressure gauge was connected upstream to read the gas pressure. Gas-flow through the densified array was measured by a downstream bubble flow meter (M-1, A. P. Buck, Inc.) with the exhaust line at atmospheric pressure. Different single-gases (H_2, N_2, and CO_2) were tested.

The height and local alignment of the CNTs within each array as well as the distribution of Fe catalyst particles on the blank samples was assessed using field emission SEM (Zeiss Ultra plus). The middle section of each CNT array was chosen as a representative section. The average CNT diameter was obtained from high resolution TEM (Philips CM120 Biofilter) measurements of 50 tubes within each array. Additional details of the CNTs in each array were obtained using TEM. The crystallinity of the CNTs was characterized by Raman spectroscopy using a Renishaw Raman with a HeNe laser at 633 nm excitation. The pore size distribution of the as-prepared CNT array was analyzed by N_2 adsorption isotherms using Barret−Joyner−Halenda (BJH) model at 77 K (Quantachrome Autosorb).

SAXS was used to investigate macroscopically the structure and alignment of the CNT arrays. SAXS data were gained on the SAXS/WAXS beamline at Australian Synchrotron using a 12 keV beam (wavelength of 1.0322 Å), and along with a 1.578 m camera length, gave data in the q range of 0.006 − 0.4 $Å^{-1}$. The beam passed through the CNT array in an orientation parallel to the substrate (Figure 2), with a beam size of approximately 50 μm in height and 75 μm in width. The scattering intensities for each sample were normalized relative to each other by accounting for the size of the sample that the beam passed through. Data were analyzed using the scatterBrain and

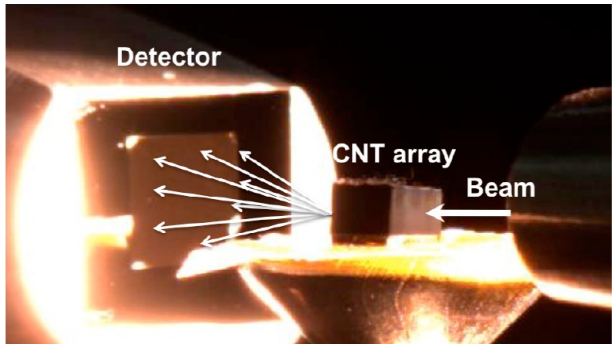

Figure 2. Experimental setup for SAXS measurement of the CNT arrays.

dx.doi.org/10.1021/am3032579 | ACS Appl. Mater. Interfaces 2013, 5, 3063−3070

the saxs15id software,[24] enabling quantification of the CNT array alignment.

RESULTS AND DISCUSSION

SEM analysis shows that without H_2 pretreatment of the catalyst-substrate prior to CNT growth the CNT array is only

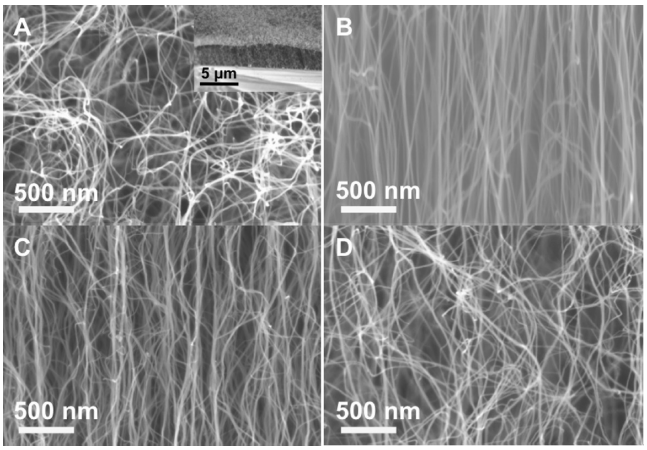

Figure 3. Typical side-view SEM images of the CNT arrays grown on catalyst without pretreatment (inset of A) and pretreated in H_2 at 750 °C for (A) 5, (B) 10, (C) 15, and (D) 20 min.

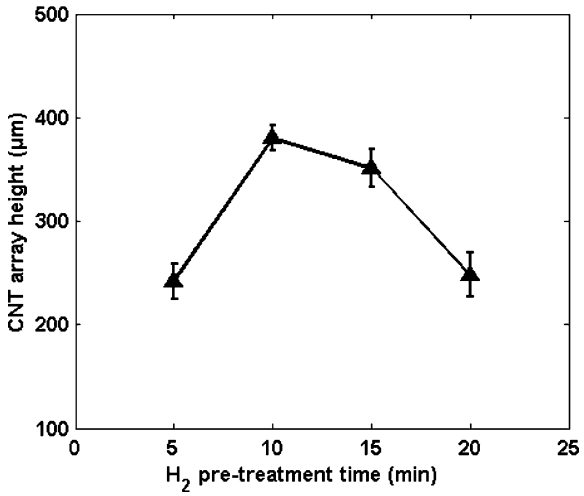

Figure 4. CNT array height, determined using SEM measurements, as a function of H_2 pretreatment time.

~2 μm high and suffers from significant entanglement (inset of Figure 3A). Annealing in a H_2-rich atmosphere affects both the height and alignment of the as-synthesized CNT arrays, with higher and better aligned CNTs achieved after annealing, relative to the CNT arrays grown on untreated catalysts. The relationship between the duration of catalyst pretreatment in H_2 and array height is shown in Figure 4. The CNT array produced on catalysts pretreated for 5 min (T5) grew to a thickness of 242 ± 17 μm, increasing to the maximum obtained CNT height of 380 ± 12 μm after 10 min (T10). Further increase in pretreatment time resulted in a decrease from the maximum height to 351 ± 18 μm after 15 min (T15) and to 247 ± 21 μm after 20 min (T20), the latter height being similar to that obtained using the 5 min catalyst pretreatment time (T5). The middle section of each array was examined using SEM to assess locally the CNT alignment (Figure 3). By visual

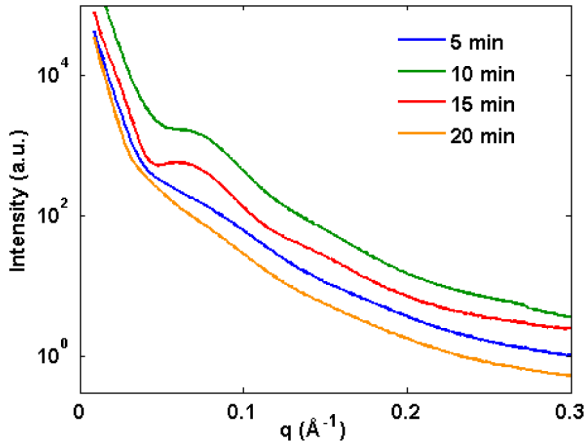

Figure 5. SAXS intensities as a function of scattering vector (reduced data: 1D patterns) for CNT arrays grown after 5–20 min H_2 pretreatment. Intensities are normalized between each array relative to the amount of sample in the beam.

inspection, the alignment observed using SEM is qualitatively worse for the T5 and T20 samples (Figures 3A and 3D, respectively) and relatively better for the T10 and T15 samples (Figures 3B and 3C, respectively). The SEM images for the T10 sample indicates particularly straight CNTs that are oriented perpendicular to the substrate.

SAXS was used to quantify the alignment and construction of the CNT arrays. Figure 5 shows the scattering intensities as a function of q at the central section of each array. Samples exhibiting a higher scattering intensity, T10 and T15, have a higher CNT areal density.[22] This is confirmed by our SEM images (Figure 3), in which T10 and T15 show significantly more CNTs per unit area. Figure 5 also reveals significantly broad features for the T10 and T15 arrays, one that is well-defined, at low q (~0.05 Å^{-1}), and another at higher q (~0.15 Å^{-1}), in contrast to the T5 and T20 arrays which exhibit no such features. The main, well-defined feature in the SAXS data obtained for the T10 and T15 samples was evaluated by fitting a Gaussian function between q = 0.03 and 0.2, allowing derivation of the peak center and width (Table 1), that are used to obtain the length scale (d) and distribution for the correlation length, respectively. Previous work has attributed the correlation length obtained from the main feature in the SAXS data of aligned CNT arrays to the diameter of the CNT walls, which correlates well to the CNT outer diameter as measured using TEM.[19] The broad feature at higher q can be attributed to the small separation distance between CNTs in the CNT bundle occasionally observed in the array, where the aligned CNTs are relatively close to each other. Some CNT arrays exhibit CNT diameters that are similar to the separation distance between CNTs, and both of these potentially contribute to the main SAX feature, although in previous work, the CNT separation distance was large enough to push scattering arising from this correlation to lower q than that arising from the CNT diameter.[25]

SEM analysis of the CNTs in the arrays studied here reveals a wide range of separation distances between CNTs, with relatively few distances that correspond to the CNT diameter. The d obtained for T10 and T15 is close to the TEM-determined average CNT diameter (Table 1). Figure 6 shows the correlation length (d, the Gaussian center) and distribution (Gaussian width) for T10 and T15 as a function of CNT array

dx.doi.org/10.1021/am3032579 | ACS Appl. Mater. Interfaces 2013, 5, 3063–3070

Table 1. q and d for the Broad Peak Observed in the 1D SAXS Data for T10 and T15 CNT Arrays, Compared with the Average CNT Diameter for 50 Tubes Obtained from TEM, and the Size of Catalyst Particles before Introducing the Carbon Source as Measured Using SEM

CNT array	pretreatment time (min)	peak position (Å^{-1})	peak width	d (nm)	CNT diameter (TEM, nm)	catalyst particles (nm)
T5	5				10.4 ± 1.8	30.7 ± 4.5
T10	10	0.059 ± 0.006	0.046 ± 0.001	10.6 ± 1.0	11.1 ± 1.9	33.2 ± 3.4
T15	15	0.057 ± 0.002	0.049 ± 0.001	11.0 ± 0.4	12.6 ± 1.6	37.1 ± 4.6
T20	20				12.9 ± 1.6	44.9 ± 7.4

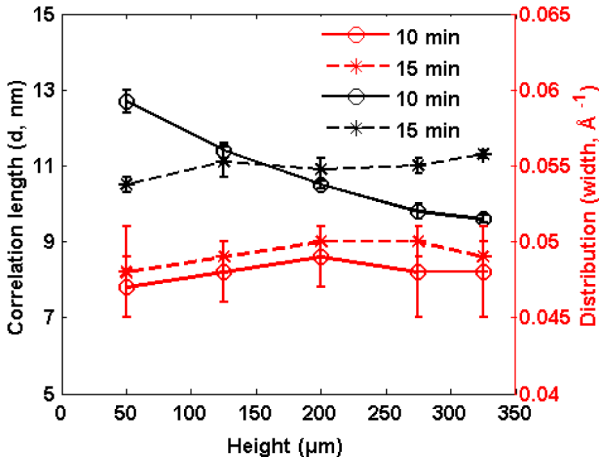

Figure 6. (d) Correlation length and distribution calculated from a Gaussian fitting to the broad feature in the 1D SAXS data (peak center and width, respectively) at different heights in the T10 and T15 CNT arrays.

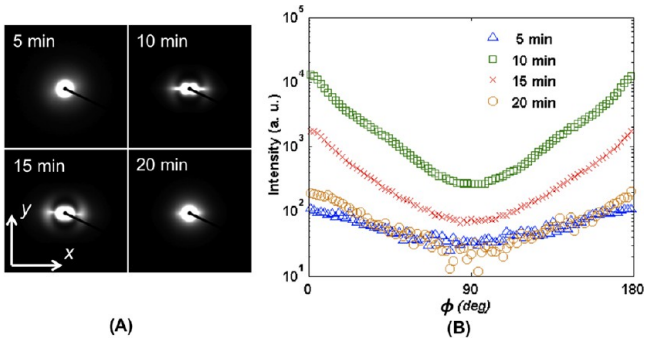

Figure 7. SAXS patterns of CNT arrays produced using different pretreatment times. (A) Typical 2D SAXS patterns. (B) Azimuthal distribution of scattered intensity at q = 0.06 Å^{-1}.

height. The distribution of d remains the same along the height of the array for both T10 and T15 arrays, however, the average d changes significantly as a function of height, particularly for the T10 array. Previous work using SAXS to assess the vertical alignment CNT arrays showed that the diameter of the CNTs, on average, is larger at the top of the film than near the substrate,[21] a result that agrees with our findings for the T15 sample. Other work revealed decreasing width of tubes with increasing height,[25] consistent with our results for the T10 sample.

Representative 2D SAXS patterns for each sample (taken from the center of the CNT array) are shown in Figure 7A. The intensity concentration in the 2D SAXS patterns at the 0 and 180° radial angle (azimuthal angle, ϕ), where 0° corresponds to the $-x$ axis, indicate vertical alignment of the CNTs,[19] such as found for T10 and T15. The better alignment of T10 and T15

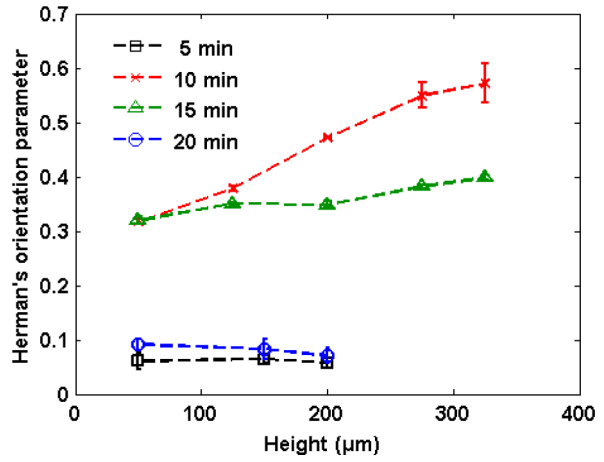

Figure 8. Herman's orientation parameter at q = 0.06 Å^{-1} obtained for SAXS data for various vertical sections of the CNT arrays produced from different pretreatment times.

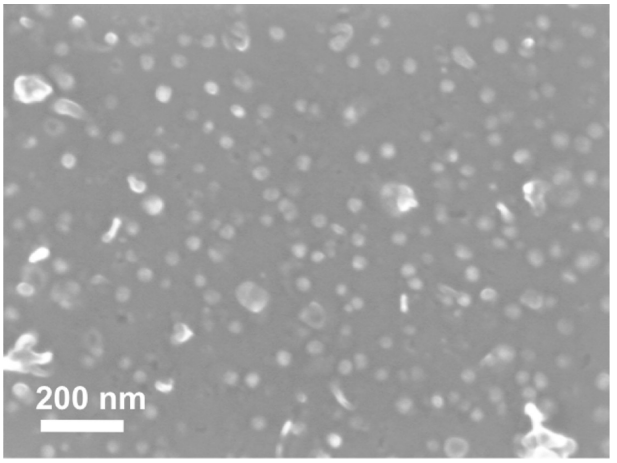

Figure 9. SEM image of the substrate surface after the CNT array (T10) prepared using a 10 min pretreatment was removed.

samples, relative to the other pretreatment times, is demonstrated by 1D azimuthal integration at q = 0.06 Å^{-1} (the correlation length for the intensity maxima for T10 and T15) (Figure 7B).

The Herman's orientation parameter, f, has been used to assess the orientation of fillers,[26] platelets,[27] and CNTs.[19] Here, we use the Herman's orientation parameter to evaluate the alignment of the CNT arrays, which is given by eqs 1 and 2:

$$f = \frac{1}{2}(3\langle\cos^2\phi\rangle - 1) \quad (1)$$

where

dx.doi.org/10.1021/am3032579 | ACS Appl. Mater. Interfaces 2013, 5, 3063−3070

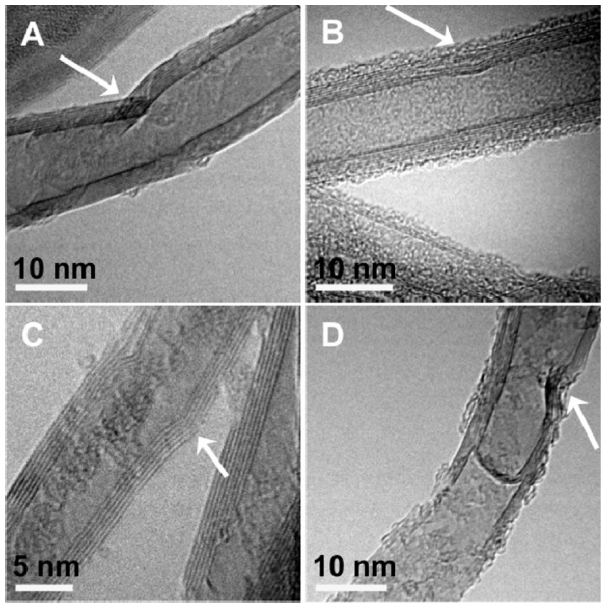

Figure 10. High-resolution TEM images of CNT arrays grown on catalyst pretreated in H_2 at 750 °C for (A) 5, (B) 10, (C) 15, and (D) 20 min. The white arrow in each image shows the location of defects.

$$\langle \cos^2 \phi \rangle = \frac{\int_0^{\pi/2} I(\phi) \sin \phi \cos^2 \phi d\phi}{\int_0^{\pi/2} I(\phi) \sin \phi d\phi} \quad (2)$$

where ϕ is the azimuthal angle and $I(\phi)$ is the SAXS intensity at an angle of ϕ. The CNTs are randomly oriented when f equals 0 and perfectly vertically or horizontally aligned when f is 1 or $-1/2$, respectively. The Herman's orientation parameter for each sample at different heights is shown in Figure 8. These results support the observations from the SEM measurements on the middle section of the CNT arrays (Figure 3), where T10, with the highest f, shows the best vertical alignment; T15 shows slightly worse alignment as consistent with the slightly lower f. Both T5 and T20 have a much lower f and are poorly aligned. Along the array, T5 and T20 showed consistently poor alignment at different heights, while T10 and 15 showed better alignment higher in the array. SEM images reveal that the CNT synthesis occurred via a base-growth mode (Figure 9), where catalyst particles were found on the substrate after peeling off the as-synthesized CNT arrays. In a base-growth mode, the top of CNTs in the arrays are synthesized before the growth of the bottom of the CNTs.[28] As the synthesis continues, the catalyst particles tend to agglomerate and be poisoned, resulting in worse alignment of the lower parts of the CNTs in the array, relative to those at the top.[19]

We conclusively demonstrate that both the height and alignment of the CNT arrays are strongly influenced by the catalyst pretreatment time, consistent with other studies.[14] As previously suggested,[14−16] heating the Fe catalyst in H_2 has several effects. The annealing promotes reduction of the thin film, which is followed by the formation of catalyst nanoparticles with diameters that increase with pretreatment time because of Ostwald ripening.[29] This process is evidenced by the increasing catalyst particle size and average CNT diameter, measured using SEM and TEM respectively, with increasing pretreatment time (Table 1). The ratio of the CNT diameter to catalyst size is similar to that previously reported using similar CVD process.[16,23] The difference between the particle size and the CNT diameter is likely caused by coarsening of the catalyst particles during cooling.[23] Ostwald ripening can be inhibited by the addition of weak oxidants,[29] which does not occur for our samples which are prepared under oxidant-free conditions. The tall and well-aligned CNT arrays achieved for samples T10 and T15 suggests that a catalyst particle size and distribution that is favorable for the production of well-aligned CNT arrays is achieved after H_2 pretreatment at 750 °C for 10 to 15 min.

TEM images (Figure 10) reveal that a thin amorphous carbon film covers the outside wall of the CNTs in the arrays. The amorphous carbon is generally produced from the self-decomposition of ethylene in an oxidant-free CVD system.[30] Defects are seen along the CNT wall, with annular rather than point defects (Figure 10B and 10C). Large defect can result in breakage of the CNT wall (Figure 10A, 10D), where the CNT direction of growth is changed at the deformation point. Relatively small defects are observed in the inner or outer CNT wall of well-aligned arrays T10 and T15 (Figure 10B, 10C) and have a negligible effect on the direction of CNT growth.

We use Raman spectroscopy to investigate CNT quality and purity, and Raman spectra of the CNTs are shown in Figure 11A. Their characteristic features include D-band intensity at ~1327 cm^{-1}, G-band intensity at ~1580 cm^{-1}, and D′-band intensity at ~1593 cm^{-1}.[31] The D-band is attributed to carbon impurities, mainly amorphous carbon, supporting the TEM

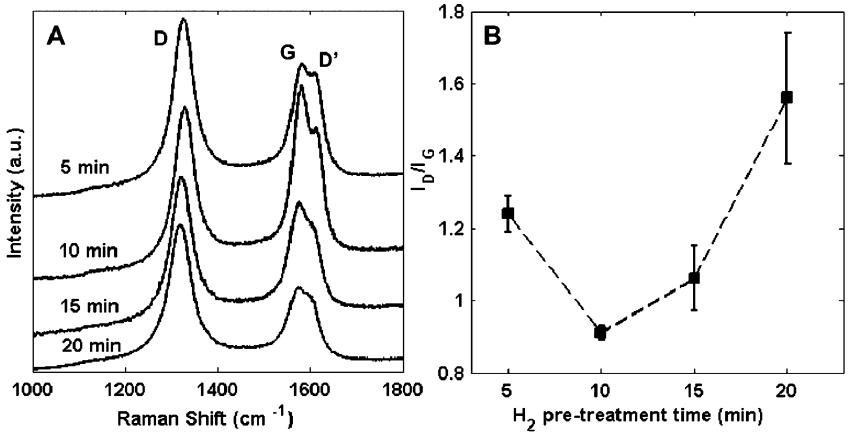

Figure 11. (A) Raman spectra of CNT arrays grown on catalyst with different H_2 pretreatment times; (B) ratio of D- to G-band intensities (I_D/I_G) as function of H_2 pretreatment time.

dx.doi.org/10.1021/am3032579 | ACS Appl. Mater. Interfaces 2013, 5, 3063−3070

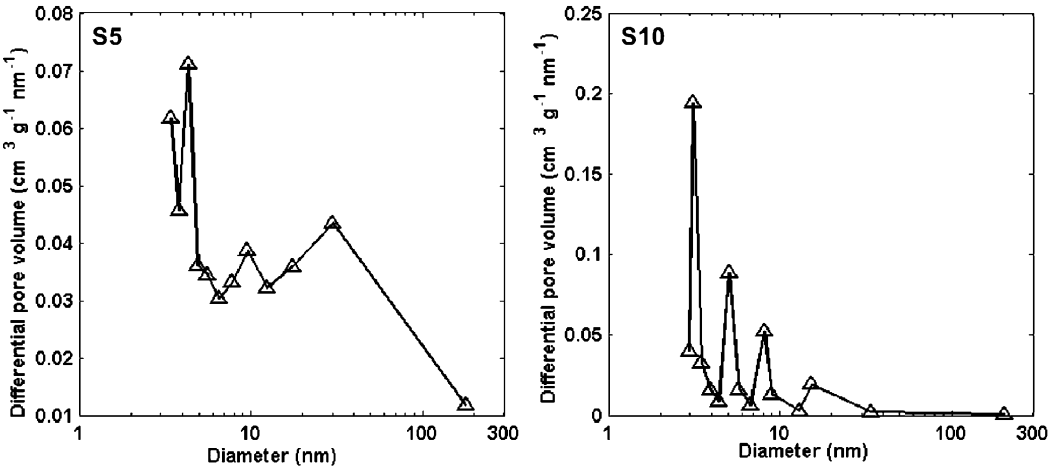

Figure 12. Pore size distributions of the densified CNT arrays prepared using 5 min (S5) and 10 min (S10) pretreatment times, calculated from N_2 adsorption at 77 K.

Table 2. Membrane Properties of the Densified CNT Arrays Prepared Using 5 min (S5) and 10 min (S10) Pretreatment Times

CNT arrays	pore size (interspacing, nm)	pore size (CNT inner diameter, nm)	porosity (%)	tortuosity
S5	27.8 ± 1.5	5.8 ± 1.2	92.4	1.35
S10	16.5 ± 1.2	6.1 ± 1.4	75.1	1.06

observations. The G- and D-band intensity ratio, I_D/I_G, has been used to assess the CNT quality,[28,32] with a I_D/I_G ratio close to unity typical for CNTs with a low degree of deformation. The I_D/I_G (Figure 11B) is 1.24 for T5, decreasing to the minimum value of 0.91 for T10, after which the ratio increases approximately linearly with pretreatment time to 1.06 for T15 and 1.56 for T20. Notably, the I_D/I_G ratio for all CNT arrays is correlated with the CNT deformation observed using TEM, and consequently, also with the array alignment determined by SEM and SAXS. The I_D/I_G is closest to unity for the T10 array, which contains CNTs with the least deformation.

According to the vapor−liquid−solid (VLS) model, the carbon feedstock is catalytically decomposed by the catalyst particles at elevated temperature, after which it dissolves into the catalyst, before finally forming CNTs when the carbon reaches supersaturation.[33] The distribution of active sites on the catalyst particle surface determines the CNT length, diameter and alignment.[34] Uniform catalyst activity is known to play an important role in the growth of aligned CNT arrays[35] and previous studies suggest that the CNT growth is primarily driven by the carbon concentration gradient in the catalyst particle.[34,36] During the stable stage of CNT growth, where carbon dissolution and precipitation rates are in equilibrium, the concentration gradient in the catalyst does not change with growth time, resulting in CNTs that are straight and relatively defect free. It has been suggested, that except for islands of catalyst optimal for CNT growth, small particles may lose CNT growth activity as a result of the overfeeding effect,[37] where Ostwald ripening minimizes surface energy[29] and small catalyst particles coalesce into larger particles. As the particle coarsening continues, the carbon concentration gradient balance in the catalyst particles is interrupted. This fluctuation of carbon concentration disturbs the CNT growth, causing the deformation of the CNTs. As the catalyst particles are distributed randomly on the substrate after annealing, smaller particles can intrude into large particles simultaneously from different directions. As a result, CNT deformation is caused by the release of the tension arising from these unequal incursions.[18] This disturbance can be offset if the smaller particles intrude with an even distribution, however, the CNT deformation will remain and form defect as a result of the fluctuation of carbon concentration in the catalyst. This hypothesis is supported by our TEM observation of annular defects, where the similar small defects are observed on each side of the CNTs in Figure 10B, 10C. As the deformation in the CNTs in our T10 and T15 arrays was balanced across the width of the CNT, the as-synthesized CNT arrays presented a higher and more aligned structure. CNT deformation can also occur under external force,[38] and if the driving force changes periodically and slowly, helical CNTs are produced.[39] In the T5 and T20 CNT arrays, the CNT deformation occurs as a result of changes in the carbon concentration, and while Ostwald ripening continues the process is repeated, resulting in

Table 3. Measured Gas Permeance (H_2, N_2, CO_2) through Densified CNT Arrays Prepared Using 5 min (S5) and 10 min (S10) Pretreatment Times, Compared with the Gas Permeance Calculated from Knudsen Diffusion and Viscous Flow

	CNT array S5	enhancement over calculation	CNT array S10	enhancement over calculation
H_2 permeance[a]	4.98 ± 0.64	8	7.56 ± 0.07	41
N_2 permeance[a]	1.61 ± 0.07	8	2.38 ± 0.05	47
CO_2 permeance[a]	1.34 ± 0.07	7	1.94 ± 0.05	48
Selectivity (H_2/N_2)	3.1		3.2	
Selectivity (H_2/CO_2)	3.7		3.9	

[a]Units: 1×10^{-5} mol Pa^{-1} m^{-2} s^{-1}.

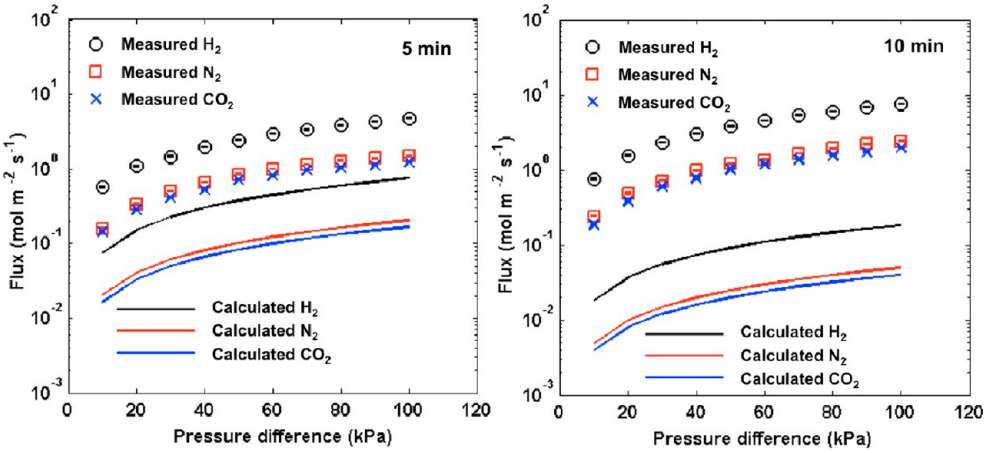

Figure 13. Comparison of the measured and the calculated gas flux through the densified CNT arrays prepared using 5 and 10 min pretreatment times, calculated on the basis of Knudsen diffusion and viscous flow.

unbalanced growth and tangled CNTs, as verified by the observation of local defects (Figure 10A, 10D). The tangled CNTs affect the growth of the surrounding CNTs and worsen the alignment in the whole array.

To assess the effect of CNT alignment on the gas transport through CNTs, we performed single-gas permeation tests using densified CNT arrays prepared under 5 and 10 min pretreatment times (relatively poorly and well-aligned arrays, respectively, as we have shown in our SEM and SAXS results). The CNT arrays for gas permeation test were grown for 120 min after 5 and 10 min pretreatment times, and are denoted by S5 and S10, respectively, with heights of 584 ± 29 μm and 1372 ± 35 μm, respectively. Yu et al. proposed that gas diffuses across the CNT array through both the inner pore of the CNTs and the interspacing between the CNTs after a shrinking process.[40] Water-etching was used to detach the aligned CNT arrays and open the CNTs.[23] The interspacings of the CNTs in S5 and S10 were calculated as 27.8 ± 1.5 nm and 16.5 ± 1.2 nm, respectively, using the mass and density of the CNTs in the array.[41,42] Another previous study showed that the pore-size distribution calculated from N_2 adsorption by the CNT arrays can be used to obtain the interspacing of CNTs in the array.[40] The pore-size distributions of the densified CNT arrays studied here (Figure 12) confirm the CNT interspacings obtained from the mass and density based calculation, where peaks in the pore-size distribution were found at ~30 and ~15 nm, for the S5 and S10 array, respectively. Using these CNT interspacings, the porosity is estimated as 92.4 and 75.1% for S5 and S10, respectively. The tortuosity is defined as the ratio of the length of the curved CNT (actual length) to that of the straight CNT distance,[43] and is 1.35 and 1.06 for S5 and S10, respectively, calculated using the SEM images. The membrane properties of the densified CNT arrays are summarized in Table 2.

Within the pore range (5−30 nm) of the S5 and S10 arrays, the gas trasport across the membrane is theoretically expected to be dominated by both Knudsen diffusion and viscous flow, as the membrane pore sizes are close to the mean free path for the gas within the membrane.[44,45] The permeance (F) is calculated as the sum of Knudsen and viscous flow (eq 3). The permeance of Knudsen flow (F_k) and viscous flow (F_v) are given in eq 4 and 5, respectively[46]

$$F = F_k + F_v \tag{3}$$

$$F_k = \frac{J_k}{\Delta P} = \frac{2}{3} r \sqrt{\frac{8RT}{\pi M}} \frac{\varepsilon}{RTL\tau} \tag{4}$$

$$F_v = \frac{1}{8} \frac{\varepsilon r^2}{LRT\mu\tau} P_m \tag{5}$$

where J_k is the Knudsen flux and ΔP is the pressure difference ε is the porosity, R is the universal gas constant, T is the absolute temperature, L is the thickness of the membrane, τ is pore tortuosity, r is the pore radius, M is molecular weight, μ is the viscosity of the gas, and P_m is the mean pressure across the membrane. H_2, N_2, and CO_2 were measured in the gas permeation tests. The measured and theoretical gas permeance are compared in Table 2. The ideal gas selectivities (H_2/N_2, H_2/CO_2) of the densified CNT arrays are close to those predicted by Knudsen diffusion, consistent with other studies.[7,40] Similar to previous studies,[40,42] the gas transport through the inner-pore of CNTs and the interspacing between the CNTs is significantly faster than the theoretical calculations. However, Table 3 and Figure 13 show that compared to the theoretical gas transport in terms of flux and permeance, the enhancement factor (~8) of the relatively poorly aligned CNT array (S5) is significantly lower than that of the well-aligned CNT array (~45 for S10). This indicates that the alignment plays an important role in enhancing the gas permeation through the densified CNT arrays. The enhancement of gas or water transport in CNT arrays over the theoretical values was explained by the smooth and frictionless surface on the CNT walls.[7] In the case of gas transport, collisions between the gas and the CNT wall are expected to be specular, with the smoothness of the wall limiting backscattering and causing the gas transport to exceed the kinetic theory.[47] Therefore, in the relatively poorly aligned CNT arrays, the pore channel available for gas transport is not perfectly straight due to the existence of defects, increasing backscattering and causing gas−gas collisions, leading to a less-enhanced gas transport.

CONCLUSIONS

Variation in the H_2 pretreatment times of the catalyst particles prior to CNT growth was conducted to optimize the height and alignment of CNT arrays. Small-angle X-ray scattering in conjunction with scanning and transmission electron microscopy enabled characterization of the CNT arrays, and in particular, quantification of their alignment and tube diameter.

We find that a 10 min pretreatment time produces the best aligned and highest CNT arrays, and that these arrays have a high areal density, relative to those produced from other pretreatment times. Analysis of the CNT quality and purity (Raman spectroscopy) and defects (transmission electron microscopy) allowed elucidation of the CNT growth mechanism. We find that the quality and purity of a CNT correlated with the appearance of defects, and consequently, with the alignment of CNTs within the array. Single-gas permeation tests on densified CNT arrays that were well- and poorly aligned indicate that the alignment of the CNT arrays significantly affects the gas transport through them. Compared to the theoretical permeance, the well-aligned densified CNT array exhibited a significantly larger enhancement (~45 times) over the theoretical permeance than that (~8 times) of the poorly aligned densified CNT array.

AUTHOR INFORMATION

Corresponding Author

*Tel: 61 2 9351 3053. Fax: 61 2 9351 2854. E-mail: xyan5399@uni.sydney.edu.au.

Notes

The authors declare no competing financial interest.

ACKNOWLEDGMENTS

X.Y. gratefully acknowledges the Australian Nuclear Science and Technology Organisation and the Chinese Scholarship Council for postgraduate research support. L.Y. acknowledges a Richard Claude Mankin postdoctoral scholarship, and A.T.H. acknowledges an ARC Future Fellowship. The authors acknowledge the facilities, and the scientific and technical assistance, of the Australian Microscopy & Microanalysis Research Facility at the Australian Centre for Microscopy and Microanalysis, The University of Sydney. We also thank Mr. V. Lo for his assistance with the SEM and high resolution TEM measurements, and Dr Y. Yin for catalyst thin film deposition, and Dr E. Carter for Raman measurement. SAXS experiments were undertaken at the SAXS/WAXS beamline at the Australian Synchrotron, Victoria, Australia.

REFERENCES

(1) Iijima, S. *Nature* **1991**, *354*, 56−58.
(2) Zhang, M.; Li, J. *Mater. Today* **2009**, *12*, 12−18.
(3) Baughman, R. H.; Zakhidov, A. A.; De Heer, W. A. *Science* **2002**, *297*, 787−792.
(4) Fan, S.; Chapline, M. G.; Franklin, N. R.; Tombler, T. W.; Cassell, A. M.; Dai, H. *Science* **1999**, *283*, 512−514.
(5) Hong, S.; Myung, S. *Nat. Nanotechnol.* **2007**, *2*, 207−208.
(6) Hinds, B. J.; Chopra, N.; Rantell, T.; Andrews, R.; Gavalas, V.; Bachas, L. G. *Science* **2004**, *303*, 62−65.
(7) Holt, J. K.; Park, H. G.; Wang, Y.; Stadermann, M.; Artyukhin, A. B.; Grigoropoulos, C. P.; Noy, A.; Bakajin, O. *Science* **2006**, *312*, 1034−1037.
(8) Liu, H.; He, J.; Tang, J.; Pang, P.; Cao, D.; Krstic, P.; Joseph, S.; Lindsay, S.; Nuckolls, C. *Science* **2009**, *327*, 64−67.
(9) Zhang, X.; Jiang, K.; Feng, C.; Liu, P.; Zhang, L.; Kong, J.; Zhang, T.; Li, Q.; Fan, S. *Adv. Mater.* **2006**, *18*, 1505−1510.
(10) Hata, K.; Futaba, D. N.; Mizuno, K.; Namai, T.; Yumura, M.; Iijima, S. *Science* **2004**, *306*, 1362−1364.
(11) Ci, L.; Manikoth, S. M.; Li, X.; Vajtai, R.; Ajayan, P. M. *Adv. Mater.* **2007**, *19*, 3300−3303.
(12) Zhao, B.; Futaba, D. N.; Yasuda, S.; Akoshima, M.; Yamada, T.; Hata, K. *ACS Nano* **2009**, *3*, 108−114.
(13) Liu, K.; Sun, Y.; Chen, L.; Feng, C.; Feng, X.; Jiang, K.; Zhao, Y.; Fan, S. *Nano Lett.* **2008**, *8*, 700−705.
(14) Nessim, G. D.; Hart, A. J.; Kim, J. S.; Acquaviva, D.; Oh, J.; Morgan, C. D.; Seita, M.; Leib, J. S.; Thompson, C. V. *Nano Lett.* **2008**, *8*, 3587−3593.
(15) Zhang, Y.; Zou, G.; Doorn, S. K.; Htoon, H.; Stan, L.; Hawley, M. E.; Sheehan, C. J.; Zhu, Y.; Jia, Q. *ACS Nano* **2009**, *3*, 2157−2162.
(16) Cui, X.; Wei, W.; Harrower, C.; Chen, W. *Carbon* **2009**, *47*, 3441−3451.
(17) Charlier, J. C. *Acc. Chem. Res.* **2002**, *35*, 1063−1069.
(18) Amelinckx, S.; Zhang, X. B.; Bernaerts, D.; Zhang, X. F.; Ivanov, V.; Nagy, J. B. *Science* **1994**, *265*, 635−637.
(19) Wang, B. N.; Bennett, R. D.; Verploegen, E.; Hart, A. J.; Cohen, R. E. *J. Phys. Chem. C* **2007**, *111*, 5859−5865.
(20) Furuta, H.; Kawaharamura, T.; Furuta, M.; Kawabata, K.; Hirao, T.; Komukai, T.; Yoshihara, K.; Shimomoto, Y.; Oguchi, T. *Appl. Phys. Express* **2011**, *3*, 15101−15103.
(21) Futaba, D. N.; Yamada, T.; Kobashi, K.; Yumura, M.; Hata, K. *J. Am. Chem. Soc.* **2011**, *133*, 5716−5719.
(22) Wang, B. N.; Bennett, R. D.; Verploegen, E.; Hart, A. J.; Cohen, R. E. *J. Phys. Chem. C* **2007**, *111*, 17933−17940.
(23) Yang, X.; Yuan, L.; Peterson, V. K.; Minett, A. I.; Yin, Y.; Harris, A. T. *ACS Appl. Mater. Interfaces* **2012**, *4*, 1417−1422.
(24) Cookson, D.; Kirby, N.; Knott, R.; Lee, M.; Schultz, D. *J. Synchrotron Radiat.* **2006**, *13*, 440−444.
(25) Ch Das, N.; Yang, K.; Liu, Y.; Sokol, P. E.; Wang, Z.; Wang, H. *J. Nanosci. Nanotechnol.* **2011**, *11*, 4995−5000.
(26) Finnigan, B.; Jack, K.; Campbell, K.; Halley, P.; Truss, R.; Casey, P.; Cookson, D.; King, S.; Martin, D. *Macromolecules* **2005**, *38*, 7386−7396.
(27) Malwitz, M. M.; Lin-Gibson, S.; Hobbie, E. K.; Butler, P. D.; Schmidt, G. *J. Polym. Sci., Part B: Polym. Phys.* **2003**, *41*, 3237−3248.
(28) Hart, A. J.; Slocum, A. H. *J. Phys. Chem. B* **2006**, *110*, 8250−8257.
(29) Amama, P. B.; Pint, C. L.; McJilton, L.; Kim, S. M.; Stach, E. A.; Murray, P. T.; Hauge, R. H.; Maruyama, B. *Nano Lett.* **2009**, *9*, 44−49.
(30) Jungen, A.; Stampfer, C.; Durrer, L.; Helbling, T.; Hierold, C. *Nanotechnology* **2007**, *18*, 075603.
(31) Dillon, A. C.; Parilla, P. A.; Alleman, J. L.; Gennett, T.; Jones, K. M.; Heben, M. J. *Chem. Phys. Lett.* **2005**, *401*, 522−528.
(32) Puretzky, A. A.; Geohegan, D. B.; Jesse, S.; Ivanov, I. N.; Eres, G. *Appl. Phys. A: Mater. Sci. Process.* **2005**, *81*, 223−240.
(33) Ding, F.; Bolton, K.; Rosen, A. *J. Phys. Chem. B* **2004**, *108*, 17369−17377.
(34) Kamachali, R. D. *Chem. Phys.* **2006**, *327*, 434−438.
(35) Huang, Z. P.; Wang, D. Z.; Wen, J. G.; Sennett, M.; Gibson, H.; Ren, Z. F. *Appl. Phys. A: Mater. Sci. Process.* **2002**, *74*, 387−391.
(36) Klinke, C.; Bonard, J. M.; Kern, K. *Phys. Rev. B: Condens. Matter Mater. Phys.* **2005**, *71*, 1−7.
(37) Lu, C.; Liu, J. *J. Phys. Chem. B* **2006**, *110*, 20254−20257.
(38) Hart, A. J.; Slocum, A. H. *Nano Lett.* **2006**, *6*, 1254−1260.
(39) Hanus, M. J.; Harris, A. T. *Carbon* **2010**, *48*, 2989−2999.
(40) Yu, M.; Funke, H. H.; Falconer, J. L.; Noble, R. D. *Nano Lett.* **2009**, *9*, 225−229.
(41) Laurent, C.; Flahaut, E.; Peigney, A. *Carbon* **2010**, *48*, 2994−2996.
(42) Yoon, D.; Lee, C.; Yun, J.; Jeon, W.; Cha, B. J.; Baik, S. *ACS Nano* **2012**, *6*, 5980−5987.
(43) Zhang, Q.; Zhou, W.; Qian, W.; Xiang, R.; Huang, J.; Wang, D.; Wei, F. *J. Phys. Chem. C* **2007**, *111*, 14638−14643.
(44) Uhlhorn, R. J. R.; Keizer, K.; Burggraaf, A. J. *J. Membr. Sci.* **1989**, *46*, 225−241.
(45) Ziarani, A. S.; Aguilera, R. *Transp. Porous Media* **2011**, 1−22.
(46) Jayaraman, V.; Lin, Y. S. *J. Membr. Sci.* **1995**, *104*, 251−262.
(47) Majumder, M.; Chopra, N.; Hinds, B. J. *ACS Nano* **2011**, *5*, 3867−3877.